Concentration enrichment, separation, and cation exchange in nano-liter-scale water-in-oil droplets

Sungu Kim[1,2], Baskar Ganapathysubramanian[2], Robbyn K. Anand[1]*

[1]Department of Chemistry, Iowa State University, 1605 Gilman Hall, 2415 Osborn Drive, Ames, IA 50011-1021

[2]Department of Mechanical Engineering, Iowa State University, 2043 Black Engineering, 2529 Union Drive, Ames, IA 50011-2030

Keywords: droplet, concentration polarization, separations, cation exchange.

ABSTRACT: Droplet-based techniques have had a profound impact in chemistry, owing to an ability to perform rapid and massively parallel reactions in minute fluid volumes. In many applications, concentration enrichment is required to increase the speed of reactions or the sensitivity of assays; but in-droplet concentration enrichment remains challenging. Here, we interface electrokinetic concentration polarization with droplet microfluidics to accomplish in-droplet de-mixing. This result is significant because the concentration of any charged species in the droplet can be enriched and the approach can be readily integrated into existing droplet workflows. Further, we show that such electrokinetic enrichment is rapid, on the order of seconds, and is robust, occurring over a wide parametric space. We further demonstrate electrokinetic separation of two anionic fluorophores within the droplet. Such a capability potentiates the droplet-templated synthesis of particles with gradient composition and the development of mobility-shift assays, which rely on discrimination of multiple species tagged with a single color fluorophore. Finally, by using a calcium-binding dye as an indicator, we demonstrate in-droplet cation exchange. This demonstration of cation exchange in droplets is significant because of its broad applicability to strategies for synthesis and bioassays. These results lay the foundation for new advanced droplet techniques with transformative applications.

Introduction

In droplet microfluidics, pico- to nanoliter-scale volumes are rapidly processed using functions that include merging, splitting and sorting, in-droplet mixing, and encapsulation of single particles.[1-4] These features have been leveraged for droplet-templated synthesis of nano- and microparticles and for highly sensitive analyses, such as single-cell enzymatic assays or digital polymerase chain reaction, which benefit from partitioning a bulk sample into thousands to millions of reaction volumes. However, following encapsulation, there are limited means by which droplet composition can be altered. This limitation is important for three reasons. First, the concentration of each reagent is critical to the reaction rate and, in assays, to signal intensity.[5,6] Therefore, there is a need for methods that enrich the concentration of reagents within a droplet. Second, in the templated synthesis of particles, a gradient in composition may be desired for applications in which two poles of the resulting particle catalyze distinct reactions.[4,7] Further, adoption of mobility-shift assays or reactions that result in a mixture of products requires a means of in-droplet separation.[8,9] Third, benchtop assays and synthetic strategies benefit from the ability to add and extract reagents and products in a controlled manner. However, the analogous functions have not been recapitulated in droplet-based workflows.

There are existing methods that accomplish concentration enrichment in the context of water-in-oil (W/O) droplets. However, these methods are limited to application prior to droplet generation[10,11] or can only sample and enrich a small fraction of the total droplet volume.[12] Enrichment of the entire droplet contents has been accomplished by evaporation[13,14] or with traveling surface acoustic waves (for droplet-confined beads),[15] but these approaches are limited in throughput and scope, respectively. Further, there is currently a dearth of methods to accomplish separation or ion exchange within droplets. There is therefore a need for rapid and universal methods to manipulate droplet composition. Here, we report a method to accomplish this goal – namely, in-droplet ion concentration polarization (ICP).

ICP is an electrokinetic phenomenon in which ionic species are locally enriched and depleted at opposing ends of an ion permselective structure[16,17] or a bipolar electrode[18,19] under a voltage bias. When propagated with two ion selective membranes in series, neighboring ion enriched and depleted zones result.[20] During ICP, the low ionic conductivity of the ion depleted zone (IDZ) leads to a strong (>10-fold) local enhancement of the electric field and the formation of concentration and electric field gradients at the IDZ boundary. The non-linear migration of ions in these gradients results in further exclusion of charged species from entering the IDZ – a feature that has been leveraged for focusing and continuous separation of charged species.[21] ICP has had a major impact in several areas of application including desalination[22-24] enrichment and separation of trace analytes[14,15,20] and bioparticles,[20,26] cellular dielectrophoresis,[27] regeneration of sensing substrates,[28] mobility shift assays for bioanalysis,[29] micelle-based extraction of uncharged compound,[30] and for the removal of excess fluid from blood.[31]

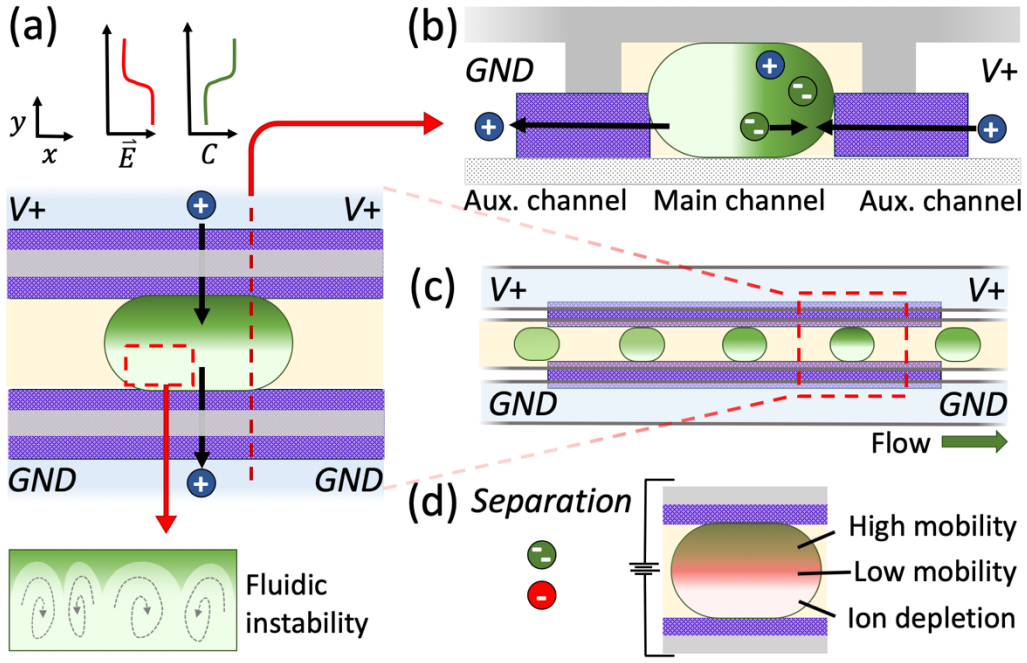

Figure 1. Illustration of enrichment and separation of charged species by concentration polarization inside W/O droplets in a microfluidic channel. (a) Top view of a droplet in ionic communication with two parallel cation selective membranes that extend into flanking electrolyte-filled auxiliary channels across which a voltage bias (V+) is applied. At top are qualitative line profiles of the electric field strength ($\vec{E}$) and the concentration of an anionic fluorophore (C) across the droplet (y-direction), illustrating that concentration is lower and the field strength higher adjacent to the cathodic membrane (GND). The inset (at bottom) is an illustration of vortex flow patterns observed in the ion depleted zone (IDZ). (b) Cross-sectional view along the cutline (dashed line) in (a). Cations are extracted from (left) and injected into (right) the droplet. Anions migrate towards the anodic membrane to maintain electroneutrality and are therefore, enriched (right). (c) Top view of a series of droplets in the main channel. The progression of concentration profiles (left to right) illustrates the gradual polarization as the droplet enters the channel segment lined by the membranes. (d) Separation of two anions having distinct electrophoretic mobilities.

We demonstrate ICP in nanoliter-scale water-in-oil (W/O) droplets for concentration enrichment and separation of charged compounds (**Figure 1**). In this method, droplets are injected into a microfluidic channel (top and side views, **Figure 1a,b**) having two thin-film cation-selective membranes patterned in parallel along the channel length. The membranes extend from underneath this main 'droplet channel' into two neighboring auxiliary channels filled with an aqueous electrolyte solution. A voltage bias applied across these auxiliary channels drives ionic current across the cation permselective membranes and through the droplets. As a result, cations are depleted from the portion of the droplet nearest the cathodic (grounded) compartment and accumulate nearer the anodic compartment. Anions within the droplet migrate away from the cathodic compartment, leaving behind an IDZ, and towards the anodic compartment where they charge pair with the accumulated cations to form an ion enriched zone (IEZ). Exemplary fluorescence microscopy images of a droplet, obtained prior to and during enrichment, along with contour lines indicating intensity, are shown in **Figure 2a-c**.

Using an anionic fluorescent tracer, we observed concentration enrichment (> 15-fold) in nanoliter-scale droplets, accompanied by vortex flow patterns in the IDZ, which are characteristic of ICP. An investigation of the impact of voltage bias and background electrolyte concentration reveals that greater maximum enrichment is achieved at higher voltage and lower ionic strength. We further show that concentration enrichment is maintained during movement of the droplets along the microchannel, and we characterize concentration profiles as a function of droplet velocity, finding that, within the investigated range of droplet velocity (< 250 μm/s), the degree of enrichment is not affected by flow. Next, we leverage this method to separate two charged fluorophores within a droplet based on their distinct electrophoretic mobilities. Finally, we exchange the cation content of a droplet for Ca^{2+}, which is evidenced by subsequent increased quantum yield of a calcium-indicator dye. In combination, the methods we introduce significantly expand the toolkit for droplet microfluidics.

Materials and Methods

Chemicals. The dianionic fluorophore (BODIPY^{2-} 4,4-Difluoro-1,3,5,7,8-pentamethyl-4-bora-3a,4a-diaza-s-indacene-2,6-disulfonic acid) were obtained from Molecular Probes (Eugene, OR). ABIL® EM 90 was obtained from Evonik Industries (Essen, Germany). All other solutions were made with reagent grade chemicals (Fisher Scientific, Waltham, MA) and diluted with double deionized water (18.2 MΩ·cm, Sartorius Arium Pro, Göttingen, Germany) before use to desired concentration. Sodium phosphate buffer at pH 7.3 was used to fill the auxiliary channel and dispersed (droplet) phase at the concentration indicated in the Results section. For the continuous phase, heavy mineral oil with 0.1 w/w% of Triton®-X100 and 3 w/w% of ABIL® EM 90 was used.

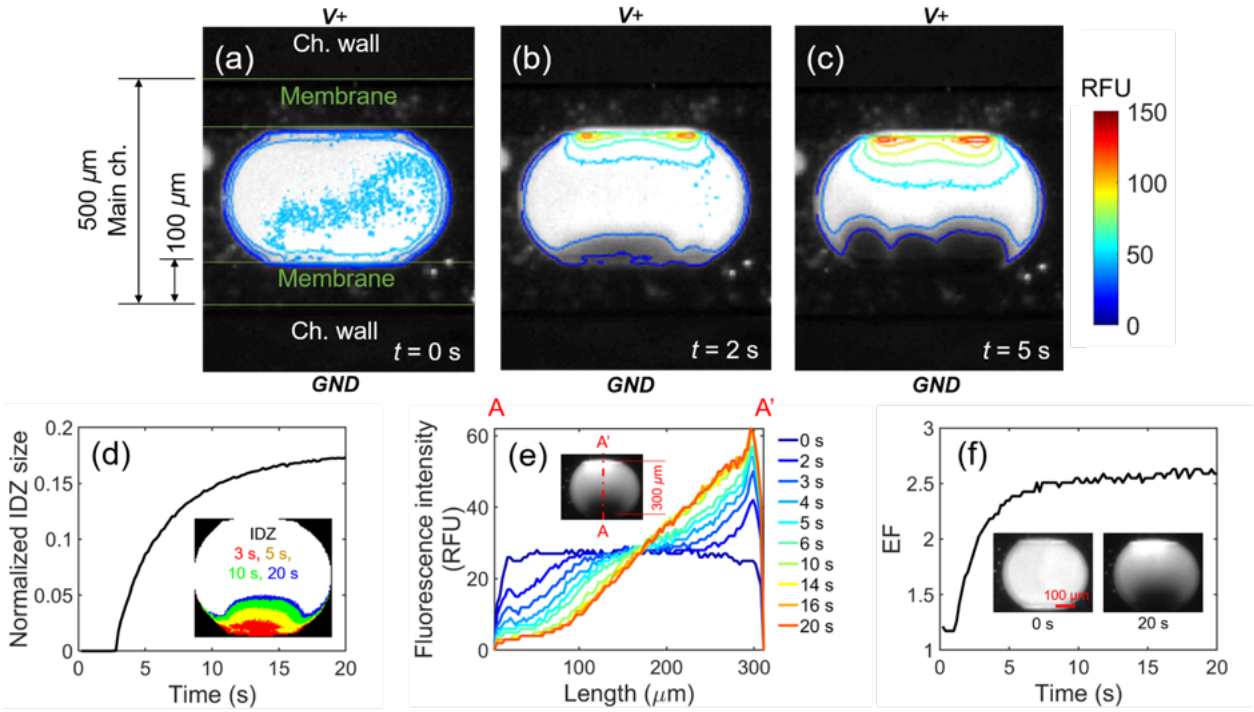

Figure 2. Electrokinetics of standing droplet enrichment. Fluorescence micrographs showing the temporal evolution of the distribution of an anionic fluorescent tracer ($BODIPY^{2-}$) at (a) t = 0 s, (b) 2 s, and (c) 5 s after initiation of an applied voltage of $V+$ = 15.0 V, in 10 mM phosphate buffer (pH 7.3). Overlaid isometric contours are included to highlight the enriched area inside the droplet. Vortex flow cause the 'scalloped' IDZ boundary depicted in (c). The volume of the droplet is 6.4 nL. De-mixing is quantified in (d-f), which show (d) IDZ area relative to the droplet area (top view), (e) fluorescence intensity along the droplet centerline (across the channel width), and (f) evolution of enrichment factor (EF) over time. In (d-f), the droplet volume is 4.6 nL and $V+$ = 4.0 V.

Poly(dimethylsiloxane) (Sylgard 184 elastomer kit, Dow Corning Corp., Midland, MI) was used for device fabrication. Platinum electrodes (99.95%) were purchased from Strem Chemicals (Newburyport, MD). Nafion perfluorinated resin (20 wt% solution in lower aliphatic alcohols) was purchased from Sigma-Aldrich (St. Louis, MO) and used as received. Rhod-2, Tripotassium Salt, cell impermeant was used as a calcium indicator.

Device Fabrication. The hybrid PDMS/glass microfluidic devices were fabricated by a previously published procedure.[32] First, 2 μm- to 8 μm-thick Nafion membranes (400 μm wide, 6.0 mm long, and spaced 300 μm apart) were deposited on a glass slide by flow patterning.[33] Next, three parallel microfluidic channels were fabricated from PDMS. The central 'main microchannel' was 10.0 mm long, 500 μm wide, and 50.0 μm tall spanning a 1.0 mm-diameter inlet and outlet. The two flanking auxiliary channels were separated from the main channel by a 250 μm-thick wall and had were 5.0 mm long, 500 μm wide, and 50.0 μm tall with 4.0 mm-diameter reservoirs at each end. Finally, the PDMS and the glass slide were exposed to an O_2 plasma (60 W, PDC-001, Harrick Plasma, Ithaca, NY) for 60 s and then bonded together. The droplet channel was aligned parallel to the Nafion strips and centered on the midpoint between them (**Scheme S1**). The assembled device was then baked at 95°C for 10 min to improve bonding. Finally, the main channel was filled with the oil phase, and the auxiliary channels were filled with an aqueous electrolyte (phosphate buffer) with concentration matched to that of the droplets described for each experiment in the *Results and Discussion*.

Droplet Generation. A microfluidic droplet generator, having a nozzle geometry similar to previously reported devices,[34] was used to form droplets with volumes ranging from approximately 2.5-25.0 nL depending on the input flow rates of the two phases. The volumetric flow rates were controlled using a syringe pump (Pump 11 Pico Plus Elite, Harvard Apparatus, Holliston, MA). Droplets were collected in 1.0 mL vials before recovery and injection via 1.0 mm-OD tubing into the device employed for enrichment.

Ion Concentration Polarization. The flow of the droplet/oil emulsion into the main channel was modulated by controlling the inlet pressure with a syringe to achieve the average linear velocities indicated in the *Results and Discussion* section. A driving voltage was applied across the device using a DC power supply (Model 6487, Keithley Picoammeter, Tektronix Inc., Beaverton, OR) connected to Pt wires positioned in both reservoirs of each the upper ($V+$) and lower (*Gnd*) auxiliary channels. The voltages employed for individual experiments are indicated in the *Results and Discussion* section.

Fluorescence Measurements. All fluorescence measurements were performed using an Eclipse Ti-S inverted fluorescence microscope (Nikon Industries, New York, NY) equipped with a digital camera (Orca-4.0, Hamamatsu Corp., Bridgewater, NJ). All images were obtained using NISElements 4.6 software (Nikon). Videos were recorded with a frame rate of 5 fps. In the case of in-droplet separation of two fluorescent tracer dyes, individual images were taken at the times indicated in the *Results and Discussion* section. Enrichment factor was calculated as the fold increase in concentration of the fluorescent tracer ($BODIPY^{2-}$) as determined by comparing the maximum fluorescence to that obtained prior to the application of the driving voltage.

Image processing. The recorded video (.avi) files were converted into sequential images using ImageJ 1.51. Further image processing was carried out in MATLAB R2017b. To define the projected area of the entire droplet and the IDZ, first, the sequential images were converted to gray scale. Next, image opening and closing[35,36] were performed on the first image (at t = 0 s) to determine a droplet boundary that excluded neighboring droplets. From a binarized the image, the equivalent diameter was measured, and the droplet mask was created enabling one-by-one image processing on a droplet. The average fluorescence intensity in a droplet, before concentration polarization, was obtained by dividing the total intensity by the area of the droplet. For the rest of the frames (t > 0 s), the maximum intensity was divided by the initial average intensity to obtain the EF. For the separation experiment, local EF was defined by dividing the instantaneous intensity at each pixel by its initial intensity (at t = 0 s). Then, the value was window averaged to minimize the contribution of the pixel noise to EF. The IDZ was defined as all of the pixels in a droplet having an intensity less than 50% of the initial average intensity. Mass conservation inside a droplet was confirmed by monitoring the total intensity of the droplet for each frame. For droplets evaluated under flowing conditions, the position of the center of the droplet was compared between frames to measure its instantaneous velocity.

Results and Discussion

Concentration Polarization in a Stationary Water-in-Oil Droplet. We first investigate the electrokinetics of charged species in standing droplets. **Figure 2a-c** is a time series of fluorescence micrographs of a droplet (approx. 6.4 nL), containing 10.0 mM phosphate buffer and 10.0 μM $BODIPY^{2-}$, an anionic fluorophore, following application of 15.0 V (at t = 0 s) to the reservoirs of the anodic auxiliary channel (V+), and ground to the cathodic auxiliary channel (*GND*). Once the voltage bias was applied, a gradient in fluorescence intensity was observed to develop across the droplet. This concentration gradient results from cation selective ionic current through the membranes contacting the droplet, which leads to high concentration (IEZ) adjacent to the anodic membrane and depletion (IDZ) at the cathodic end. This result is important because it demonstrates that there is ionic communication between the droplet and the membranes, which leads to concentration polarization. Our findings further imply that ions are either transported across the oil layer, which surrounds the droplet, or that the droplet wets the membrane. The latter mechanism is likely since the membrane is primed by hydrating it in the aqueous electrolyte prior to the experiment.

The integral of fluorescence intensity across the droplet was monitored over time to verify conservation of the fluorophore in the droplet. The maximum variation in this integral was calculated for each droplet in all experiments included in this study, and the mean variation in these values was 3.8±0.3% (**Figure S1**, Supporting Information, SI). This result supports our conclusion that the observed concentration polarization is due to redistribution of the fluorophore within the droplet, and not leakage, photobleaching, or local shift in pH.

Figure 2a-c illustrates the temporal evolution of the concentration profile in the ion depleted and enriched zones. Isometric contour lines are overlaid on top of the fluorescence images to aid in visualization. Two local maxima developed at the ends of the line of contact between the droplet and the anodic membrane (red lines, **Figure 2c**), where the electric field strength is expected to be greatest. The IDZ boundary developed an irregular shape due to the presence of fluid vortices (illustrated in **Figure 1a**, inset). This fluidic instability has been attributed to electro- and diffusio- osmosis driven, respectively, by the steep gradients in electric field strength and ion concentration found there.[37,38] Collectively, these features of the concentration profile provide strong evidence of ICP as the underlying mechanism for enrichment.

The temporal evolution of ICP in a standing droplet is further characterized by plotting the normalized IDZ size (**Figure 2d**), concentration profile (**Figure 2e**), and enrichment factor (EF) - defined as the maximum 'fold' enrichment in the concentration of the dye (**Figure 2f**). For a detailed description of how these variables are calculated, see the SI. The composition of the droplet evaluated (**Figure 2d-f**) is the same as in the previous experiment (**Figure 2a-c**), but the volume (2.5 nL) and applied voltage (4.0 V) are reduced. To evaluate the normalized IDZ size, we first defined the IDZ area by setting a threshold at one half of the spatially averaged intensity within the droplet. Image pixels having intensities below this threshold were considered to be part of the IDZ area, which was then normalized to total droplet area. **Figure 2d** shows that the normalized IDZ size increased rapidly within the first 10 s following initiation of a voltage bias, then approached an asymptote at 0.17 (17% of the droplet) at 20 s. The inset of **Figure 2d** further illustrates the growth of the IDZ (shaded region) in the droplet over time.

Figure 2e shows the evolution of the intensity profile along the droplet centerline (parallel to the electric field). A concentration gradient develops rapidly and then approaches a steady state (t > 10 s), exhibiting a distinctive characteristic of droplet enrichment. This behavior contrasts that of conventional enrichment by ICP in a single phase, where a shockwave-like concentration gradient propagates upstream without interruption.[39] The spatially constrained ICP presented here allows for manipulation of charged compounds in an individual droplet without disturbing the continuous phase (oil) or other droplets. Another notable feature of the concentration profile is that it is nearly linear and, under these conditions (low voltage), extends across the entire width of the droplet, which leads to just over 2.5-fold enrichment. Results obtained at higher voltages (**Figures S2-S5**) display steeper gradients and an IDZ boundary extending past the equator of the droplet, thereby enabling greater enrichment.

Figure 2f shows that EF increased rapidly over the first 5 s, then reaches its maximum value of 2.5 at t = 10 s. Unlike conventional ICP-based enrichment, in which electrostatic repulsion of a charged species, such as an analyte, from the IDZ is balanced by convection, here there is not a continuous flux of this species from upstream (instead, repulsion is balanced by geometric confinement). For this reason, isolation of species within a droplet presents both a disadvantage, namely, limited enrichment, and an important advantage in many chemical and biological systems. First, there is often meaningful spatiotemporal variation in the composition of the input sample stream, such as when monitoring cell secretions or the effluent of a chromatographic or electrophoretic separation.[40,41] In such a case, enrichment prior to droplet encapsulation[10,11] would lead to loss of information. Second, each droplet may contain distinct entities, such as individual cells or nanoparticles.

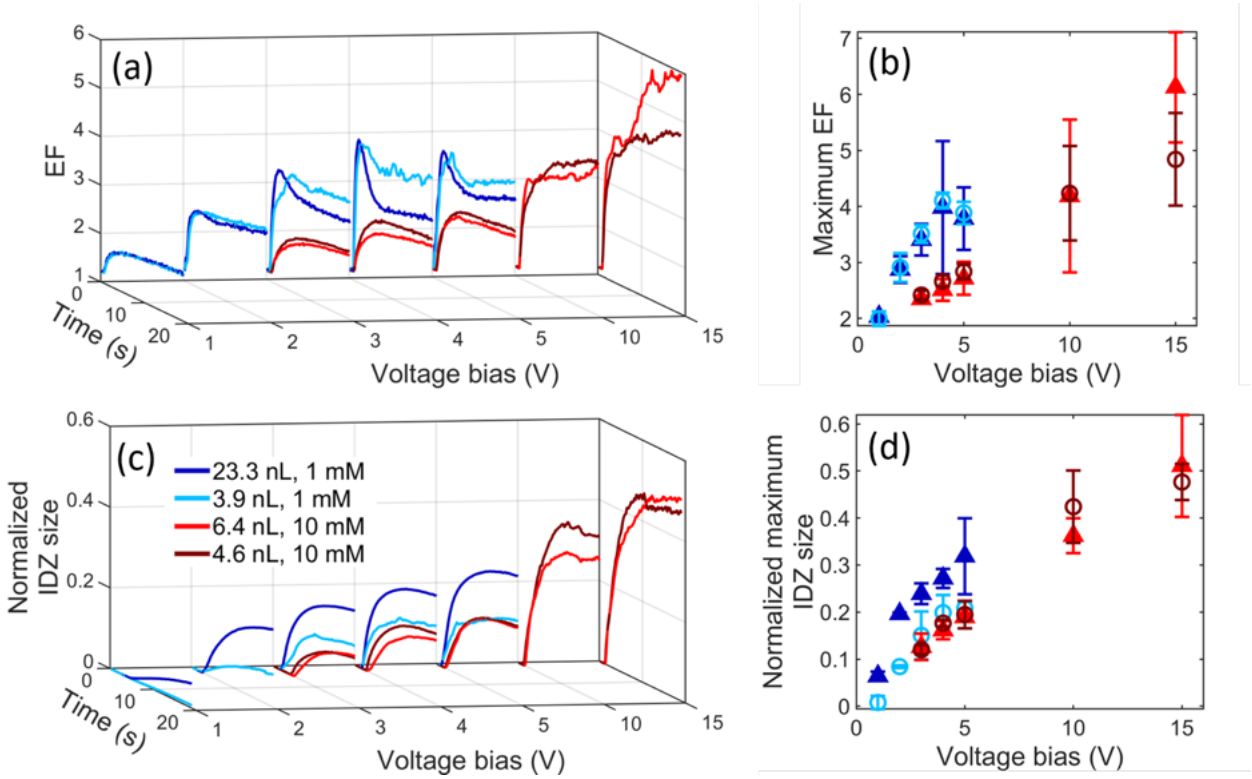

Figure 3. (a) Plot of the EF over time, and at several voltage biases, for four distinct droplets having the volumes and buffer concentrations indicated ($n = 3$). (b) Maximum EF (limiting value) as a function of the voltage bias applied during the experiments shown in (a). All droplets contained 10.0 μM $BODIPY^{2-}$, in addition to 1.0 mM phosphate buffer for 23.3 nL (dark blue triangles) and 3.9 nL (light blue circles) and 10.0 mM phosphate buffer for 6.4 nL (light red triangles) and 4.6 nL (dark red circles). (c) Plot of normalized IDZ size for the same experiments as evaluated in (a). (d) Normalized maximum IDZ size (limiting value from (c)) plotted for each voltage bias. The error bars show the 95% confidence level.

Finally, confinement is a key feature of certain processes, as in the formation of crystallites or nanoscale materials, processes which could be augmented by enrichment.

Factors Impacting the Spatiotemporal Evolution of Concentration Profiles during In-Droplet ICP. We next investigated three experimental parameters that impact the spatiotemporal evolution of the concentration distribution of the anionic fluorophore - namely, the electrolyte concentration, the magnitude of the applied voltage bias, and droplet size. For each of two buffer concentrations (1.0 and 10.0 mM phosphate buffer, pH 7.3) two droplets with distinct volumes were evaluated over a range of voltages (V+, 1.0 to 15.0 V). At each condition, the ICP experiment was performed in triplicate.

Figure 3a shows the temporal evolution of EF, plotted as an ensemble average for each triplicate. In all cases, there is an initial rapid increase in EF (from t = 0 to 5 s), which then approaches a limiting value. The limiting EF and enrichment rate are positively correlated to voltage bias and negatively correlated to ionic strength. In **Figure 3b**, the maximum EF, plotted as a function of voltage bias for each set of conditions (droplet volume and buffer concentration), follows similar trends.

Ouyang et al. attribute the limit of enrichment, in a single phase, to two distinct mechanisms.[21] In the electrokinetic (EK) limit, an electric field gradient is defined by the dominant electrolyte species, and low abundance charged compounds (e.g., analytes) are focused by counterbalancing convection and electromigration at a specific electric field strength. In this scenario, having a high electrolyte concentration compared to that of the compounds to be enriched is key to achieving high EF because when their concentration approaches that of the electrolyte, the electric field gradient is locally damped. This phenomenon defines the electrokinetic limit.[21] In the alternative mechanism, the limit is defined by the role that the enriched compound plays in maintaining electroneutrality (called the NT limit). In this case, this charged compound carries a significant fraction of the ionic current. This fraction is increased at lower electrolyte concentration, which leads to a higher limiting EF. The result of **Figure 3a** - namely, the negative correlation between the EF limit and electrolyte (phosphate buffer) concentration - implies that the in-droplet ICP reported here is governed by the NT mechanism. Further experimental investigation, aided by computational studies, is required to verify this attribution and to identify the boundaries of the NT regime.

Another critical feature of the enrichment transient is that, in larger droplets (dark blue trace, **Figure 3a**), EF peaks early (at approx. 2.5 s) and then decays to a lower steady value. We hypothesize that this disruption of the enrichment process is caused by the development of larger and more numerous vortices, leading to mixing, within a greater droplet volume. The onset of this fluidic instability is gradual, which explains the delayed decay in EF. Our interpretation builds upon reported suppression of vortices under geometric confinement.[42] As a measure of the efficiency of enrichment, we further evaluated the fraction of the droplet occupied by the IDZ, which is expected to be positively correlated to EF. **Figure 3c,d** show the projected area of the IDZ (defined as for **Figure 2d**) normalized to that of the entire droplet. By comparing IDZ

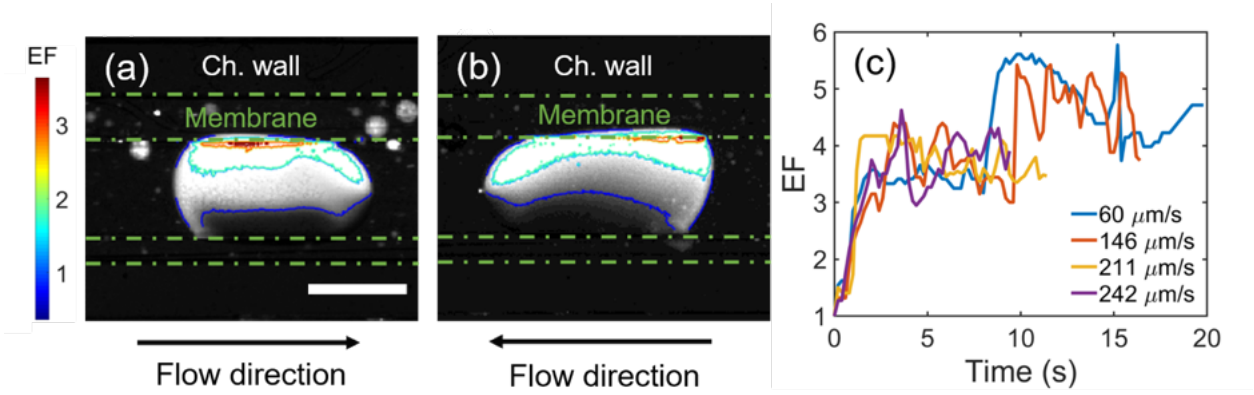

Figure 4. In-droplet ICP under flowing conditions. Fluorescence micrographs showing the distribution of an anionic fluorophore during enrichment at $V+$ = 10.0 V in droplets subjected to pressure driven flow at an average linear velocity of (a) 210 μm/s and (b) 241 μm/s. Droplets were comprised of 10.0 μM $BODIPY^{2-}$ in 1.0 mM phosphate buffer (pH 7.3). Note the shape of each IDZ is distorted due to fluid circulation in the droplet. (c) Plot of EF as a function of time at four distinct droplet velocities. Consistent enrichment was achieved over a wide range of droplet speed. The scale bar length is 300 μm.

size to EF (**Figure 3a**) for matched droplets, it is apparent that a larger IDZ corresponds to higher EF, except in the largest droplet (23.3 nL, dark blue trace, **Figure 3c,d**), which implies that the efficiency of ICP is diminished. Taken together, the results of **Figure 3** predict maximum enrichment in smaller droplets, under higher voltage, and at low ionic strength.

Concentration Profiles During In-Droplet ICP Under Flowing Conditions. While stationary droplets provide a simple system for the characterization of electrokinetics in droplets, many applications of droplet microfluidics require continuous fluid flow. Therefore, we next evaluated the impact of flow on enrichment. **Figures 4a** and **4b** are fluorescence micrographs showing the distribution of the anionic tracer ($BODIPY^{2-}$) during in-droplet ICP under pressure driven flow. To obtain this result, droplets comprising 10.0 μM $BODIPY^{2-}$ in 1.0 mM phosphate buffer, were flowed into the channel at an average linear velocity of 210 μm/s (left to right, **Figure 4a**) and 241 μm/s (right to left, **Figure 4b**); then, a voltage bias of 10.0 V was applied; finally, the images were obtained at t = 5 s and 9 s, respectively. From these images, it is apparent that the IDZ is distorted by the fluid flow and becomes asymmetrical. However, there is no gross mixing of the contents. This lack of mixing between the upper and lower halves can be attributed to known fluidic patterns that develop in flowing droplets - separate circulating flows develop in each half.[43] This result confirms that enrichment can be maintained during flow.

Figure 4c shows temporal evolution of EF observed at several fluid velocities. The maximum EFs were 3- to 5-fold, which is comparable to those obtained under similar conditions in stationary droplets (dark red trace at 10.0 V, **Figure 3a**), which supports our conclusion that mixing between the IDZ and IEZ is insignificant. The fluctuation in EF as the droplet moves along the channel is attributed to irregularity of the surface of the cation selective membranes, leading to 'hot' and 'cold' spots, where the ionic current is higher and lower, respectively. This finding underscores the importance of reliable methods for fabricating reproducible and uniform ion permselective structures for the advancement of in-droplet ICP.

In-Droplet Separation of Charged Compounds with Distinct Electrophoretic Mobilities. Finally, we investigated the ability of in-droplet ICP to accomplish separation of multiple charged compounds having distinct electrophoretic mobilities. ICP-based separation has been demonstrated extensively in a single phase.[29,44,45] The mechanism of separation in these prior reports is counter-flow focusing, in which pressure-driven or electroosmotic flow balances electromigration of the compounds at distinct axial locations, dictated by their mobilities, along a fluidic channel. While sustained unidirectional flow is absent within droplets, we hypothesized that separation could still occur, driven by the interplay of migration, diffusion, and geometric confinement.

Figures 5 and **S6** show the results obtained during in-droplet ICP of two anionic tracers having higher ($BODIPY^{2-}$, green) and lower (Texas Red, red) mobility, relative to each other. In this experiment, stationary droplets comprising 10.0 μM $BODIPY^{2-}$, 10 μM Texas Red, and 10 mM phosphate buffer (pH 7.3) were subjected to $V+$ = 10.0 V, and images of green (**Figure 5b**) and red (**Figure 5c**) fluorescence were obtained after 10 s. An overlay of the brightfield images of each droplet with red and green fluorescence (**Figure 5a**) show three distinct regions - depletion of both dyes (bottom, cathodic end), red dye only (middle), and both dyes together (top, anodic end). This partial separation is linked to a greater degree of confinement for the higher mobility (green) species due to relatively stronger migration away from the IDZ. Plots of the local 'fold' enrichment (local EF) for each dye along the droplet centerline (**Figure 5d** and **Figure S6d,h** in SI) provide a more quantitative view of the concentration profiles. For both tracers, the highest local enrichment factor was found near the anodic membrane. The peak EF of $BODIPY^{2-}$ was 5 times larger than for Texas Red, and the concentration gradient was steeper. From the separate images of $BODIPY^{2-}$ (**Figure 5b**) and Texas Red (**Figure 5c**), and contour plots (**Figure 5e,f**) it is clear that there are different tiers of tracer enrichment. The separation of the tracers is more distinct when their radial distribution is considered. Finally, the penetration of Texas Red into the IDZ ('fingers' of dye in **Figure 5c**) demonstrates the mobility dependence of the instability.[46] The practical implication of this finding is that low mobility compounds will undergo less efficient enrichment.

We anticipate that sharper transitions and separation of more than two species can be accomplished following further optimization of the experimental conditions. We further expect that a deeper understanding of the concentration profiles will allow for the deconvolution fluorescence intensity traces obtained for multiple species with a single fluorescence

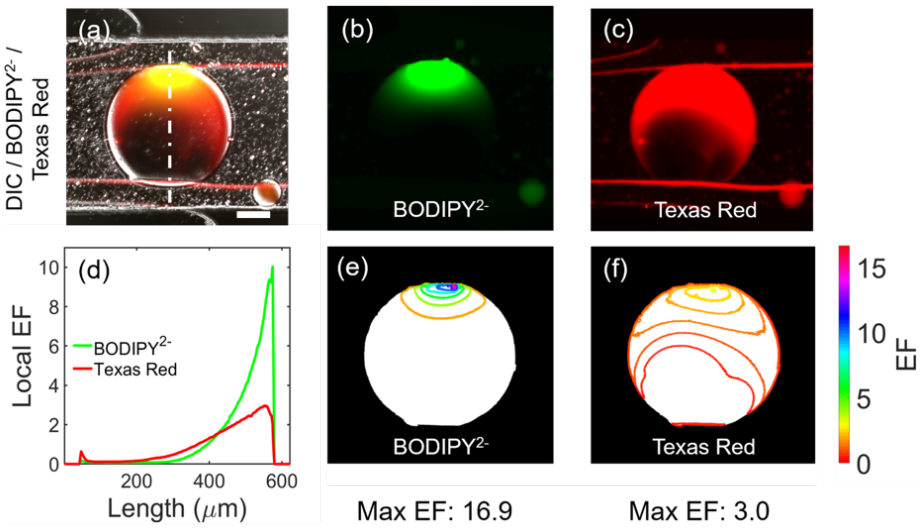

Figure 5. In-droplet separation of fluorescent tracers with distinct electrophoretic mobilities. (a) Overlaid and images of differential interference contrast (DIC, bright field) with fluorescence images showing the distributions of (b) the green tracer ($BODIPY^{2-}$) and (c) red tracer (Texas Red). (d) A plot of the local EF for each of these two tracers along the cutline in (a). (e and f) Contour lines that map the distribution of each tracer as a function of local EF. The droplet analyzed here contained 10.0 mM phosphate buffer (pH 7.3), 10.0 μM $BODIPY^{2-}$, and 10.0 μM Texas Red. The droplet volume was 5.50 nL. $V+ = 10.0$ V. The scale bar is 100 μm.

wavelength. These findings are significant because electrokinetic separation in droplets promises to enable single-color ratiometric methods, such as mobility-shift assays[29,45] and fractionation prior to droplet splitting, thereby revolutionizing droplet microfluidics.

Electrokinetically-Driven Cation Exchange in Water-in-Oil Droplets. Finally, we demonstrate cation injection into droplets from the anodic auxiliary channel via the ion permselective membrane. The droplet depicted in the fluorescence images of **Figure 6a** contained 10.0 μM calcium indicator dye (Rhod-2) and 10.0 mM Tris buffer (pH 8.0). In two successive experiments, the anodic auxiliary channel contained, first, 10.0 mM Tris buffer and then 10.0 mM $CaCl_2$. In both cases, upon application of $V+ = 5.0$ V, the calcium indicator was enriched at the anodic membrane and depleted at the cathodic membrane (middle row in **Figure 6a**). After 30 min of operation, with Tris buffer in the anodic auxiliary channel, the intensity of the calcium indicator was unchanged (compare first and last row, right column, **Figure 6a**). In contrast, in the presence of $CaCl_2$ in the auxiliary channel, the fluorescence of the calcium indicator increased (left column, **Figure 6a**). Fluorescence images showing a longer segment of the channel show three droplets undergoing this process in parallel (**Figure S7**). This result demonstrates the transport of Ca^{2+} from the auxiliary channel into the droplet. This injection of cations must be balanced by removal of an equivalent quantity of charge from the droplet via the cathodic membrane, and therefore, this method also provides a means for selective ion extraction from droplets. We further observed distinct morphologies of the IDZ in the two cases (center row, **Figure 6a**), which is attributed to altered mobility of the indicator between its bound and unbound states. Upon binding Ca^{2+}, the indicator decreases in net charge from 3^- to 1^-, which results in a lower mobility and corresponding smaller IDZ size. These results are consistent with those observed during separation of species with distinct mobilities (**Figure 5**).

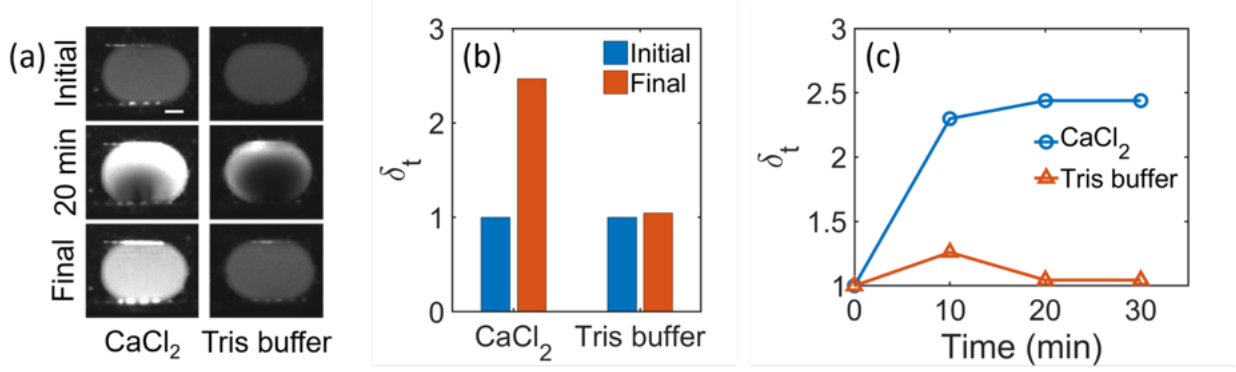

Figure 6. An increase in the fluorescence of a calcium indicator dye confirms the transport of Ca^{2+} cations from the auxiliary channel to the droplet. Initially, the droplet contained 10.0 μM Rhod-2 (indicator) in 10.0 mM Tris buffer. In successive experiments, the anodic auxiliary channel contained, first, 10.0 mM Tris buffer and then, 10.0 mM $CaCl_2$. (a) Droplet images obtained before, during ($t = 20$ min), and 5 min after applying a voltage bias ($V+ = 5.0$ V) for 30 min in the presence (left column) and absence (right column) of Ca^{2+} in the anodic auxiliary channel. (b) Normalized intensity variation (δ_t) before and after each of these experiments. (c) Variation of δ_t over the duration of the experiments.

The change in intensity due to Ca^{2+} injection was quantified and the normalized total intensity of the droplet $\boldsymbol{\delta}_t$ (defined in more detail in the SI) are compared for the initial and final states of both cases (**Figure 6b**) and as a function of time (**Figure 6c**). After the injection of Ca^{2+}, the indicator intensity increased by 2.5 fold, while there was no significant change in intensity in the absence of Ca^{2+}. The intensity approaches a limiting value in approximately 10 min, which is consistent with complete displacement of the initial $TrisH^+$ content of the droplet (about 5 μC of ionic charge) at a rate of several nanoamperes of ionic current. This magnitude of current is typical for ICP at an ion selective membrane with a similar cross sectional area in contact with an aqueous electrolyte solution. Monitoring the ion exchange current in W/O droplets is a promising avenue to achieve more refined control over droplet composition and will be the focus of future studies. These results are significant because they demonstrate modification of droplet composition '*on the fly*', without alteration of droplet volume. Further, the magnitude of the ion selective current, as controlled by the applied voltage and the serial resistances of the membranes and droplet, control the rate at which ionic charge is injected. Finally, the results provide further fundamental support for the mechanism illustrated by **Figure 1**.

Conclusion

We have presented a microfluidic approach for electrokinetically-driven concentration polarization and cation exchange in nanoliter-scale W/O droplets. This development advances droplet microfluidics by allowing rapid and tunable control of solute distribution within droplets, thereby influencing the speed and sensitivity of bioassays and allowing separation for both analysis and synthesis of particles with graded composition. Further, cation exchange has the potential to allow addition and extraction of reagents and products from the droplet volume in a way that is analogous to benchtop techniques, and importantly, the rate and total dose are controlled here by the magnitude and duration of the applied voltage. Our results clearly demonstrate electrokinetically-driven de-mixing of charged species confined to droplets. A quantitative characterization of the in-growth of the IDZ, the temporal evolution of the distribution of a fluorescent tracer, and its resulting degree of enrichment as a function of experimental parameters (droplet volume, voltage, ionic strength) predicts stronger enrichment in smaller droplets due to increased fluidic stability and reveals that the role of the tracer in maintaining electroneutrality is a potential mechanism for the limitation of enrichment in droplets. These findings provide guidance for further enhancement of in-droplet ICP, which promises to provide an order-of-magnitude decrease in limits of detection and reaction time. We further show that ICP-induced enrichment is maintained in droplets subjected to pressure driven flow, which is important for the successful integration of this method into existing droplet workflows. Additionally, we have shown that ICP in droplets containing two anionic tracers, having distinct mobilities, leads to the development of three separate segments - consisting of neither, one, and both compounds - along the path of ionic current. Finally, a simple alteration of the electrolyte composition in the anodic auxiliary channel led to cation exchange, demonstrated by increased fluorescence of a calcium indicator dye. Taken together, these results demonstrate the potential for in-droplet ICP to transform droplet microfluidics and its application in materials science and biotechnology. Our ongoing research is focused on coupled experimental and numerical studies to more clearly delineate operational regimes and the integration of in-droplet ICP with existing high-impact applications of droplets.

ASSOCIATED CONTENT

Supporting Information

The Supporting Information is available free of charge on the ACS Publications website.

The SI contains a summary of closely related techniques for interfacing concentration enrichment with droplet microfluidics (**Table S1**), a detailed procedure for device fabrication, the equations employed for data analysis, a plot of the maximum change in integrated fluorescence intensity across each droplet during ICP (**Figure S1**), plots of fluorescence intensity profiles obtained for each of the droplets included in this study (**Figures S2-S5**), the results of an additional in-droplet separation performed at a higher buffer concentration (**Figure S6**), and fluorescence images of a longer channel segment showing three droplets undergoing cation exchange in parallel (**Figure S7**). (PDF)

AUTHOR INFORMATION

Corresponding Author

* rkanand@iastate.edu

ORCID

Robbyn K. Anand: 0000-0003-2801-8280

ACKNOWLEDGMENT

Funding for this research was provided by an NSF CAREER grant awarded by the Chemistry Directorate Chemical Measurement and Imaging Program under award number 1849109.

REFERENCES

(1) Schneider, T.; Kreutz, J.; Chiu, D. T. The Potential Impact of Droplet Microfluidics in Biology. *Anal. Chem.* **2013**, *85*, 3476–3482.

(2) Guo, M. T.; Rotem, A.; Heyman, J. A.; Weitz, D. A. Droplet Microfluidics for High-Throughput Biological Assays. *Lab Chip* **2012**, *12*, 2146–2155 .

(3) Shang, L.; Cheng, Y.; Zhao, Y. Emerging Droplet Microfluidics. *Chem. Rev.* **2017**, *117*, 7964–8040.

(4) Nisisako, T. Recent Advances in Microfluidic Production of Janus Droplets and Particles. *Curr. Opin. Colloid Interface Sci.* **2016**, *25*, 1–12.

(5) Lee, J. H.; Song, Y. A.; Tannenbaum, S. R.; Han, J. Increase of Reaction Rate and Sensitivity of Low Abundance Enzyme Assay Using Micro/Nanofluidic Preconcentration Chip. *Anal. Chem.* **2008**, *80*, 3198–3204.

(6) Jeong, H. .; Cosgrove, B. D.; Lauffenburger, D. A.; Han, J. Microfluidic Concentration-Enhanced Cellular Kinase Activity Assay. *J. Am. Chem. Soc.* **2009**, *131*, 10340–10341.

(7) Shang, L.; Cheng, Y.; Zhao, Y. Emerging Droplet Microfluidics. *Chem. Rev.* **2017**, *117*, 7964–8040.

(8) Cheow, L. F.; Sarkar, A.; Kolitz, S.; Lauffenburger, D.; Han, J. Detecting Kinase Activities from Single Cell Lysate Using Concentration-Enhanced Mobility Shift Assay. *Anal. Chem.* **2014**, *86*, 7455–7462.

(9) Cheow, L. F.; Han, J. Continuous Signal Enhancement for Sensitive Aptamer Affinity Probe Electrophoresis Assay Using Electrokinetic Concentration. *Anal. Chem.* **2014**, *86*, 7455–7462.

(10) Yu, M.; Hou, Y.; Zhou, H.; Yao, S. An on-Demand Nanofluidic Concentrator. *Lab Chip* **2015**, *15*, 1524–1532.

(11) Chen, C.-H.; Sarkar, A.; Song, Y.-A.; Miller, M. A.; Kim, S. J.; Griffith, L. G.; Lauffenburger, D. A.; Han, J. Enhancing Protease Activity Assay in Droplet-Based Microfluidics Using a Biomolecule Concentrator. *J. Am. Chem. Soc.* **2011**, *133*, 10368–10371.

(12) Sanghavi, B. J.; Varhue, W.; Chávez, J. L.; Chou, C.-F.; Swami, N. S. Electrokinetic Preconcentration and Detection of Neuropeptides at Patterned Graphene-Modified Electrodes in a Nanochannel. *Anal. Chem.* **2014**, *86*, 4120–4125.

(13) Petersson, M.; Nilsson, J.; Wallman, L.; Laurell, T.; Johansson, J.; Nilsson, S. Sample Enrichment in a Single Levitated Droplet for Capillary Electrophoresis. *J. Chromatogr. B Biomed. Sci. Appl.* **1998**, *714*, 39–46.

(14) He, M.; Sun, C.; Chiu, D. T. Concentrating Solutes and Nanoparticles within Individual Aqueous Microdroplets. *Anal. Chem.* **2004**, *76*, 1222–1227.

(15) Park, K.; Park, J.; Jung, J. H.; Destgeer, G.; Ahmed, H.; Sung, H. J. In-Droplet Microparticle Separation Using Travelling Surface Acoustic Wave. *Biomicrofluidics* **2017**, *11*, 064112.

(16) Li, M.; Anand, R. K. Recent Advancements in Ion Concentration Polarization. *Analyst* **2016**, *141*, 3496–3510.

(17) Wang, Y.-C.; Stevens, A. L.; Han, J. Million-Fold Preconcentration of Proteins and Peptides by Nanofluidic Filter. *Anal. Chem.* **2005**, *77*, 4293–4299.

(18) Perdue, R. K.; Laws, D. R.; Hlushkou, D.; Tallarek, U.; Crooks, R. M. Bipolar Electrode Focusing: The Effect of Current and Electric Field on Concentration Enrichment. *Anal. Chem.* **2009**, *81*, 10149–10155.

(19) Anand, R. K.; Sheridan, E.; Knust, K. N.; Crooks, R. M. Bipolar Electrode Focusing: Faradaic Ion Concentration Polarization. *Anal. Chem.* **2011**, *83*, 2351–2358.

(20) Kwak, R.; Kang, J. Y.; Kim, T. S. Spatiotemporally Defining Biomolecule Preconcentration by Merging Ion Concentration Polarization. *Anal. Chem.* **2016**, *88*, 988–996.

(21) Ouyang, W.; Ye, X.; Li, Z.; Han, J. Deciphering Ion Concentration Polarization-Based Electrokinetic Molecular Concentration at the Micro-Nanofluidic Interface: Theoretical Limits and Scaling Laws. *Nanoscale* **2018**, *10*, 15187–15194.

(22) MacDonald, B. D.; Gong, M. M.; Zhang, P.; Sinton, D. Out-of-Plane Ion Concentration Polarization for Scalable Water Desalination. *Lab Chip* **2014**, *14*, 681–685.

(23) Oh, Y.; Lee, H.; Son, S. Y.; Kim, S. J.; Kim, P. Capillarity Ion Concentration Polarization for Spontaneous Biomolecular Preconcentration Mechanism. *Biomicrofluidics* **2016**, *10*, 014102.

(24) Kim, S. J.; Ko, S. H.; Kang, K. H.; Han, J. Direct Seawater Desalination by Ion Concentration Polarization. *Nat. Nanotechnol.* **2010**, *5*, 297–301.

(25) Jeon, H.; Lee, H.; Kang, K. H.; Lim, G. Ion Concentration Polarization-Based Continuous Separation Device Using Electrical Repulsion in the Depletion Region. *Sci. Rep.* **2013**, *3*, 3483.

(26) Kwak, R.; Kim, S. J.; Han, J. Continuous-Flow Biomolecule and Cell Concentrator by Ion Concentration Polarization. *Anal. Chem.* **2011**, *83*, 7348–7355.

(27) Anand, R. K.; Johnson, E. S.; Chiu, D. T. Negative Dielectrophoretic Capture and Repulsion of Single Cells at a Bipolar Electrode: The Impact of Faradaic Ion Enrichment and Depletion. *J. Am. Chem. Soc.* **2015**, *137*, 776–783.

(28) Phan, D.-T.; Jin, L.; Wustoni, S.; Chen, C.-H. Buffer-Free Integrative Nanofluidic Device for Real-Time Continuous Flow Bioassays by Ion Concentration Polarization. *Lab Chip* **2018**, *18*, 574–584.

(29) Cheow, L. F.; Sarkar, A.; Kolitz, S.; Lauffenburger, D.; Han, J. Detecting Kinase Activities from Single Cell Lysate Using Concentration-Enhanced Mobility Shift Assay. *Anal. Chem.* **2014**, *86*, 7455–7462.

(30) Berzina, B.; Anand, R. K. Continuous Micellar Electrokinetic Focusing of Neutral Species Driven by Ion Concentration Polarization. *Lab Chip* **2019**, *19*, 2233–2240.

(31) Berzina, B.; Anand, R. K. An Electrokinetic Separation Route to Source Dialysate from Excess Fluid in Blood. *Anal. Chem.* **2018**, *90*, 3720–3726.

(32) McDonald, J. C.; Duffy, D. C.; Anderson, J. R.; Chiu, D. T.; Wu, H.; Schueller, O. J.; Whitesides, G. M. Fabrication of microfluidic systems in poly(dimethylsiloxane). *Electrophoresis* **2000**, *21*, 27–40.

(33) Lee, J. H.; Song, Y.-A.; Han, J. Multiplexed proteomic sample preconcentration device using surface-patterned ion-selective membrane. *Lab Chip* **2008**, *8*, 596–601.

(34) Hatch, A. C.; Fisher, J. S.; Tovar, A. R.; Hsieh, A. T.; Lin, R.; Pentoney, S. L.; Yang, D. L.; Lee, A. P. 1-Million droplet array with wide-field fluorescence imaging for digital PCR. *Lab Chip* **2011**, *11*, 3838–3845.

(35) Büning, H. K.; Manna, Z.; Waldinger, R. *The logical basis for computer programming. Volume I. Deductive reasoning. Addison-Wesley series in computer science.* Addison-Wesley Publishing Company, Reading, Mass., 1985, pp. 618.

(36) Manna, Z.; Waldinger, R. *The logical basis for computer programming. Volume II. Deductive systems. Addison-Wesley series in computer science.* Addison-Wesley Publishing Company, Reading, Mass., 1990, pp. 642.

(37) Druzgalski, C. L.; Andersen, M. B.; Mani, A. Direct Numerical Simulation of Electroconvective Instability and Hydrodynamic Chaos Near an Ion-Selective Surface. *Phys. Fluids* **2013**, *25*, 110804.

(38) Cho, I.; Kim, W.; Kim, J.; Kim, H.-Y.; Lee, H.; Kim, S. J. Non-Negligible Diffusio-Osmosis Inside an Ion Concentration Polarization Layer. *Phys. Rev. Lett.* **2016**, *116*, 254501.

(39) Zangle, T. A.; Mani, A.; Santiago, J. G. On the Propagation of Concentration Polarization from Microchannel-Nanochannel Interfaces. Part II: Numerical and Experimental Study. *Langmuir* **2009**, *25*, 3909–3916.

(40) Li, X.; Hu, J.; Easley, C. J. Automated Microfluidic Droplet Sampling with Integrated, Mix-and-Read Immunoassays to Resolve Endocrine Tissue Secretion Dynamics. *Lab Chip* **2018**, *18*, 2926–2935.

(41) Bandak, B.; Yi, L.; Roper, M. G. Microfluidic-Enabled Quantitative Measurements of Insulin Release Dynamics from Single Islets of Langerhans in Response to 5-Palmitic Acid Hydroxy Stearic Acid. *Lab Chip* **2018**, *18*, 2873–2882.

(42) Kim, K.; Kim, W.; Lee, H.; Kim, S. J. Stabilization of Ion Concentration Polarization Layer Using Micro Fin Structure for High-Throughput Applications. *Nanoscale* **2017**, *9*, 3466–3475.

(43) Leong, C. M.; Gai, Y.; Tang, S. K. Y. Internal Flow in Droplets within a Concentrated Emulsion Flowing in a Microchannel. *Phys. Fluids* **2016**, *28*, 112001.

(44) Laws, D. R.; Hlushkou, D.; Perdue, R. K.; Tallarek, U.; Crooks, R. M. Bipolar Electrode Focusing: Simultaneous Concentration Enrichment and Separation in a Microfluidic Channel Containing a Bipolar Electrode. *Anal. Chem.* **2009**, *81*, 8923–8929.

(45) Cheow, L. F.; Han, J. Continuous Signal Enhancement for Sensitive Aptamer Affinity Probe Electrophoresis Assay Using Electrokinetic Concentration. *Anal. Chem.* **2011**, *83*, 7086–7093.

(46) Gao, T.; Mirzadeh, M.; Bai, P.; Conforti, K. M.; Bazant, M. Z. Active control of viscous fingering using electric fields. *Nat. Commun.* **2019** *10*, 4002.

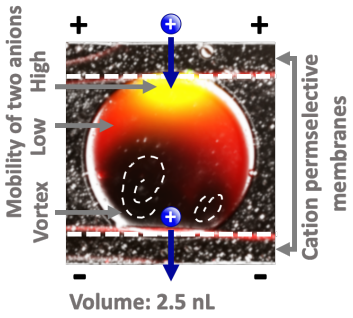
+
+
Mobility of two anions
High
Low
Vortex
Cation permselective membranes
-
-
Volume: 2.5 nL

Supporting Information

Concentration enrichment, separation, and cation exchange in nanoliter-scale water-in-oil droplets

Sungu Kim[1,2], Baskar Ganapathysubramanian[1], Robbyn K. Anand[2]*

[1]Department of Mechanical Engineering, Iowa State University, 2043 Black Engineering, 2529 Union Drive, Ames, IA 50011-2030
[2]Department of Chemistry, Iowa State University, 1605 Gilman Hall, 2415 Osborn Drive, Ames, IA 50011-1021

The integration of concentration enrichment schemes with droplet microfluidics has been previously undertaken to accomplish two goals: (1) to physically isolate locally enriched species from a bulk solution (enrichment prior to droplet formation), and (2) to enhance the detection of a target species present in a droplet (enrichment after droplet formation). **Table S1** summarizes approaches that accomplish these goals.

Table S1. Approaches that combine droplet microfluidics with concentration enrichment.

First Author	*Enrichment before/after droplet formation*	*Full contents of droplet enriched?*	*Enrichment mechanism*
Yu [1]	Before	N/A	ICP-enriched BSA sent to droplet generator
Chen [2]	Before	N/A	ICP-enriched cell lysate sent to droplet generator
Sanghavi [3]	After	No	Part of droplet enriched by ICP in nanochannel
Petersson [4]	After	Yes	Active evaporation of droplet volume
He [5]	After	Yes	Passive evaporation of droplet volume
Park [6]	After	Yes	Traveling surface acoustic waves enrich beads
This study	After	Yes	ICP of the entire contents of each droplet, spatial separation of droplet components, and cation exchange

In two of these reports, target species are enriched and separated into focused bands prior to subsequent encapsulation into droplets. This strategy was employed to 'lock in' the 10^4-fold enrichment of dye-linked bovine serum albumin (BSA) [1] and to accomplish a 10-fold reduction in assay time following the 16-fold enrichment of matrix metalloproteinases (MMPs) from diluted cellular supernatant prior to droplet encapsulation [2]. To achieve enrichment of solutes after a sample is encapsulated into droplets, Sanghavi et al. demonstrated the extraction of analytes from droplets by microdialysis and their subsequent enrichment by ICP in

nanochannels [3]. This approach allows sampling and enhanced detection of a limited portion of the droplet contents. In-droplet enrichment of solutes has been accomplished by evaporation [4,5], and more recently, traveling acoustic waves (TSAWs) were employed to enrich polystyrene beads prior to droplet splitting at a Y-junction [6]. This overview of related techniques highlights the need for a method that is capable of enrichment of a target species from the entire volume of a droplet.

Device fabrication. The device that was utilized for in-droplet ICP was constructed from a glass substrate, onto which two parallel thin film Nafion membranes were patterned, aligned with an upper PDMS monolith that defined three independent microfluidic channels. The membranes were flow-patterned on the glass substrate as follows. First, a PDMS monolith (green, **Scheme S1a**) was caste-molded on a Si wafer patterned with SU-8 2025. The PDMS was imprinted with two channels, spaced 300 μm apart measuring 6.0 mm long, 400 μm wide, and 25.0 μm tall with a 1.0 mm-diameter inlet and outlet. Second, a 25 mm x 25 mm x 1 mm glass slide was cleaned in an alkaline solution (NH_4OH:H_2O:H_2O_2, 1:1:1, at 60 ℃ for 10 min) followed by rinsing with d.d.i. water, ethanol, drying with N_2, and 60 s exposure to O_2 plasma. Third, the PDMS monolith was reversibly sealed to the glass slide. Nafion resin was pipetted on top of the inlet of each channel and then pulled through by suction applied to the outlet (**Scheme S1b**). Then, the glass slide was baked at 95 ℃ for 10 min on a hot plate to cure the Nafion (**Scheme S1c**). While curing, the Nafion shrinks to its final thickness of 2-8 μm. The PDMS channels used to pattern the membranes was peeled away leaving cured Nafion on the slide glass.

Separately, a PDMS monolith defining three microchannels (orange, **Scheme S1a**) was fabricated by soft lithography from a SU-8 2050 patterned Si wafer. The central ‘main microchannel’ was 10.0 mm long, 500 μm wide, and 50.0 μm tall spanning a 1.0 mm-diameter inlet and outlet. The two flanking auxiliary channels were separated from the main channel by a 250 μm-thick wall and had were 5.0 mm long, 500 μm wide, and 50.0 μm tall with 4.0 mm-diameter reservoirs at each end. This PDMS monolith was exposed to an O_2 plasma for 60 s. Immediately after plasma treatment, these three microchannels were aligned on top of the membranes. Finally, the device was baked at 95 ℃ for 10 min in an oven (**Scheme 1d**). Note that channels were aligned parallel to the membranes and centered on them such that each membrane spanned the wall between an auxiliary channel and the main channel. Finally, the main channel was filled with the oil phase, and the auxiliary channels were filled with an aqueous electrolyte (phosphate buffer) with concentration matched to that of the droplets described for each experiment in the *Results and Discussion*.

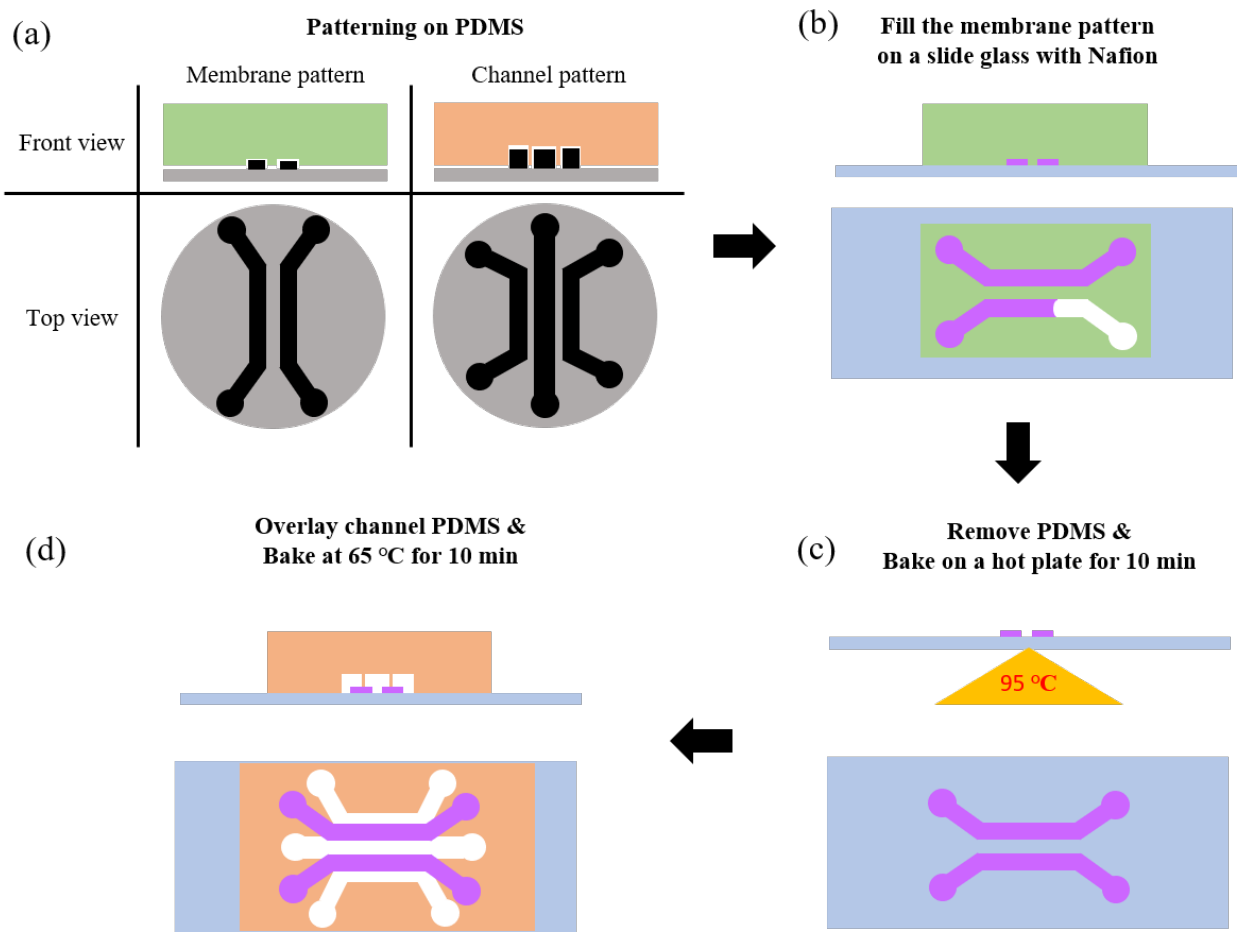

Scheme S1. Device preparation. Pattern membrane and channels on PDMS from a silicon wafer (a). Place the membrane PDMS on the slide glass, then, inject Nafion solution through punch holes (b). Bake at 95 ℃ for 10 min to cure Nafion on a hot plate and remove the PDMS (c). Align the channel PDMS chip on the membrane (d).

Conservation of mass in droplets. The W/O interface and cation selective membrane isolate anionic analytes inside a droplet. This isolation allows enrichment without loss of analyte. The variation in integrated fluorescence intensity across the droplet, δ_t, was evaluated using the following equation.

$$\delta_t = \frac{\int_{\Omega_D} I_t \, \partial\Omega_D - \int_{\Omega_D} I_0 \partial\Omega_D}{\int_{\Omega_D} I_0 \, \partial\Omega_D} \approx \frac{\sum_{i\in\Omega_D} I_{t,i} - \sum_{i\in\Omega_D} I_{0,i}}{\sum_{i\in\Omega_D} I_{0,i}} \qquad (1)$$

Here, I_t, I_0, and Ω_D are the local intensity at time t, the local intensity at $t = 0$ s, and the projected area of the droplet in the image. Subscript i represents the pixel index. **Figure S1** shows the maximum δ_t, expressed as a percentage, at several voltage biases. The variations of droplet intensity were minute with the average value 3.8±0.3%. This small variation confirms that the majority of the analyte was confined to the droplets during the enrichment.

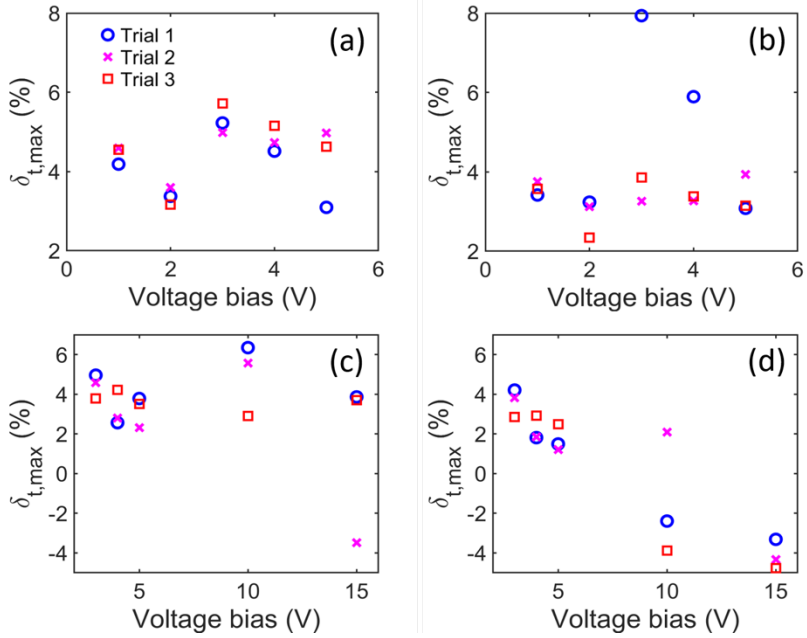

Fig. S1. The maximum percent change in integrated fluorescence, δ_t, during the enrichment of stationary droplets at several voltages; three trials each at (a) 1.0 mM phosphate buffer, 22.3 nL droplet, (b) 1.0 mM phosphate buffer, 3.9 nL droplet, (c) 10.0 mM phosphate buffer, 6.4 nL droplet, and (a) 10.0 mM phosphate buffer, 4.6 nL droplet. The negligible variation during the enrichment ensures the majority of analytes were confined inside the droplets. The mean maximum variation was 3.8±0.3%.

Evaluation of enrichment factor (EF) and normalized IDZ size. EF is the ratio between the maximum enriched concentration and the original concentration. EF was evaluated by dividing the maximum intensity in the droplet by the average droplet intensity, obtained prior to initiation of a voltage bias, where, N_D is the number of pixels in the droplet.

$$EF = \frac{\max\limits_{i\in\Omega_D} I_i}{\sum_{i\in\Omega_D} I_{0,i}/N_D} \qquad (2)$$

To evaluate the normalized IDZ size, the number of pixels in the IDZ region, N_{IDZ}, was divided by the number of pixels in the entire droplet as expressed below.

$$\frac{N_{IDZ}}{N_D} \qquad (3)$$

Intensity profile along the droplet centerline during ICP. Figures S2-S5 show the temporal evolution of the fluorescence intensity profile along the droplet centerline that lies perpendicular

to the channel axis. Each figure comprises data for a distinct droplet volume and composition. Plots (a-e) within a figure differ by voltage. Note that the location of the maximum fluorescence intensity within a droplet is frequently not located on the centerline; therefore, the intensity profiles plotted here may not reflect the calculated EF.

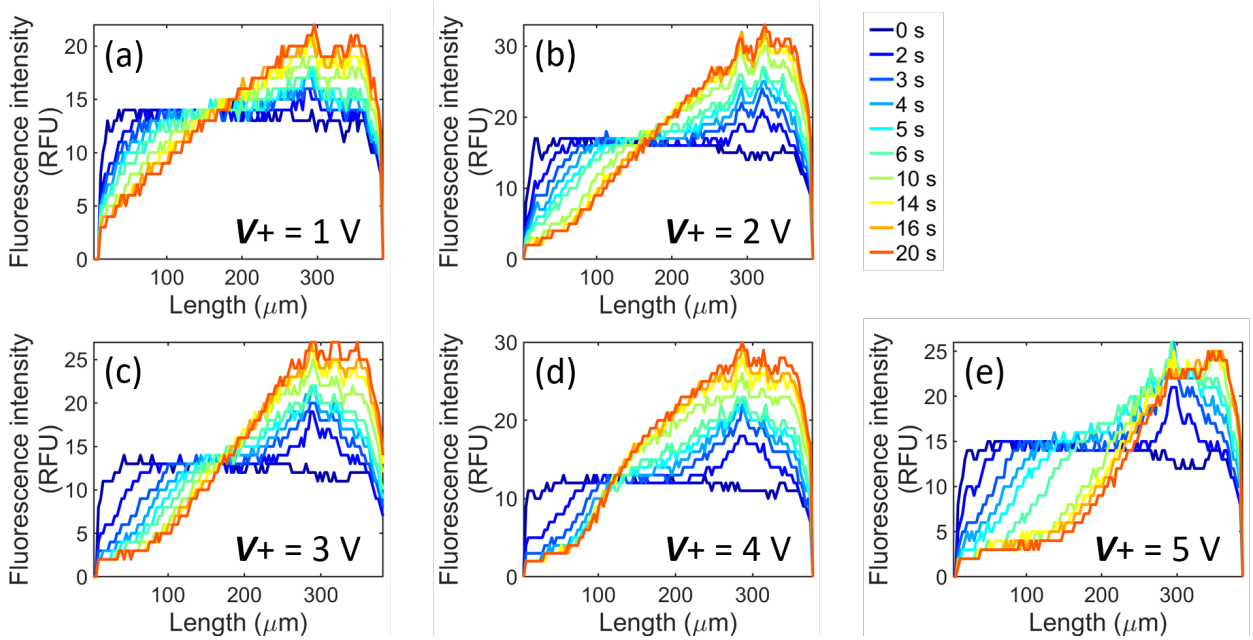

Fig. S2. Temporal evolution of the fluorescence intensity profile along the droplet centerline of a 22.3 nL droplet containing 1.0 mM phosphate buffer and 10.0 μM $BODIPY^{2-}$. The applied voltage bias was (a) 1 V, (b) 2 V, (c) 3 V, (d) 4 V, and (e) 5 V.

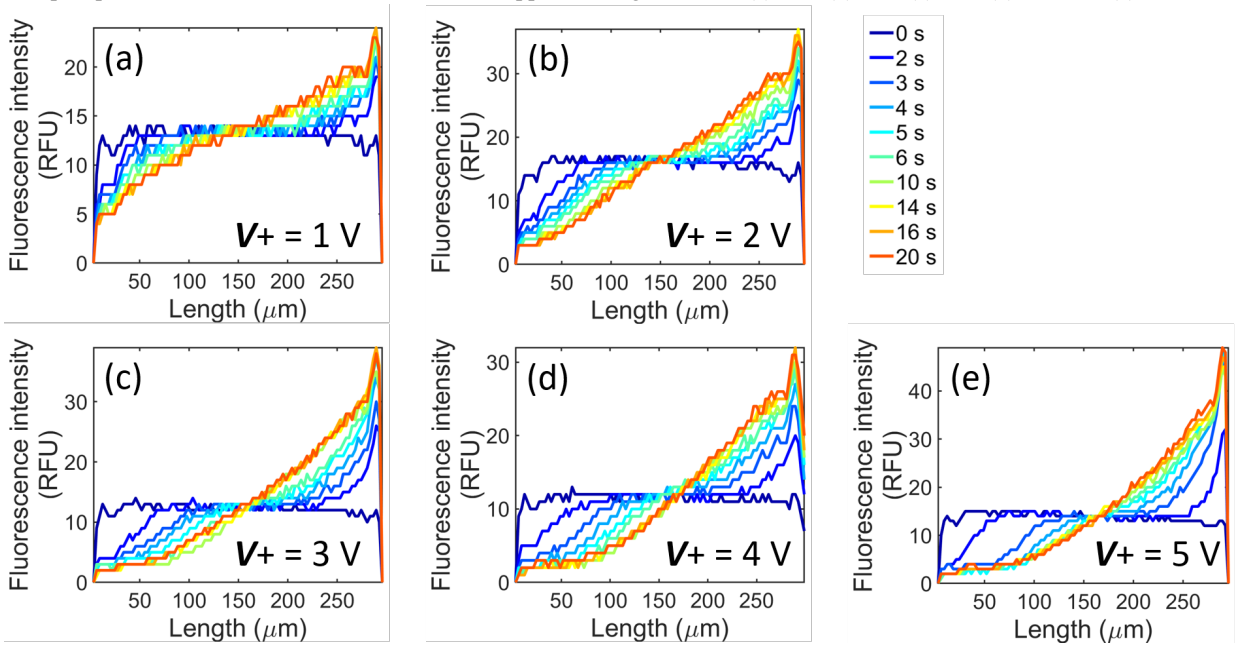

Fig. S3. Temporal evolution of the fluorescence intensity profile along the droplet centerline of a 3.9 nL droplet containing 1.0 mM phosphate buffer and 10.0 μM $BODIPY^{2-}$. The applied voltage bias was (a) 1 V, (b) 2 V, (c) 3 V, (d) 4 V, and (e) 5 V.

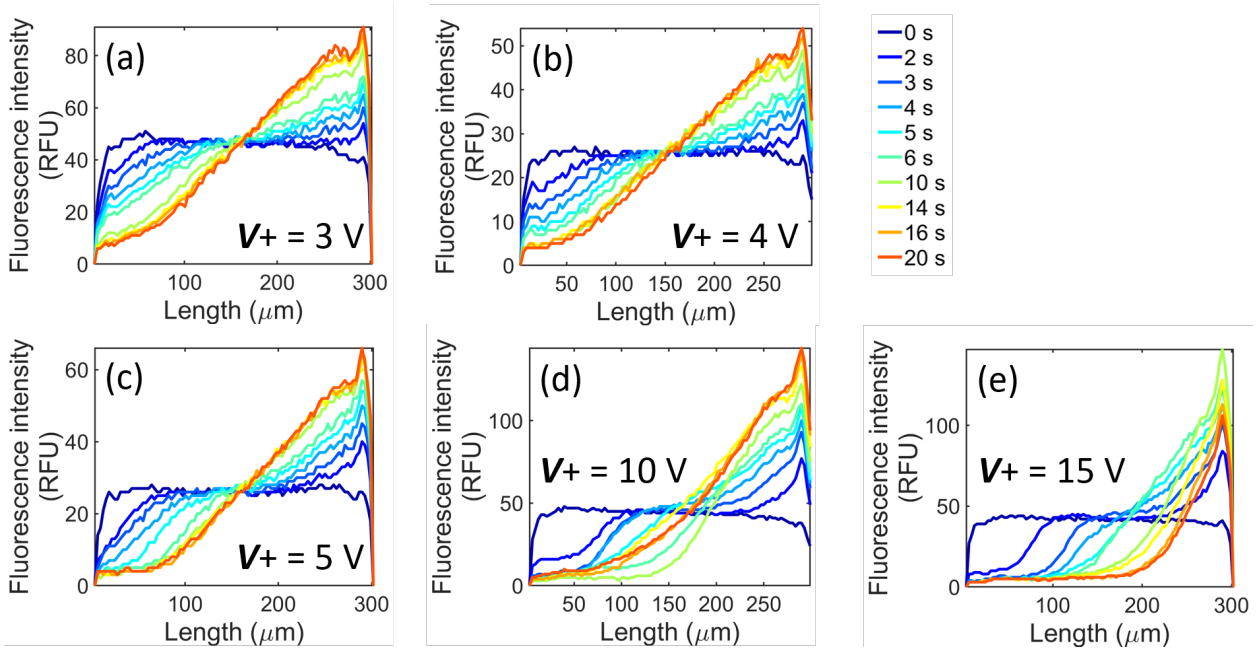

Fig. S4. Temporal evolution of the fluorescence intensity profile along the droplet centerline of a 6.4 nL droplet containing 10.0 mM phosphate buffer and 10.0 μM BODIPY^{2-}. The voltage bias was (a) 3 V, (b) 4 V, (c) 5 V, (d) 10 V, and (e) 15 V.

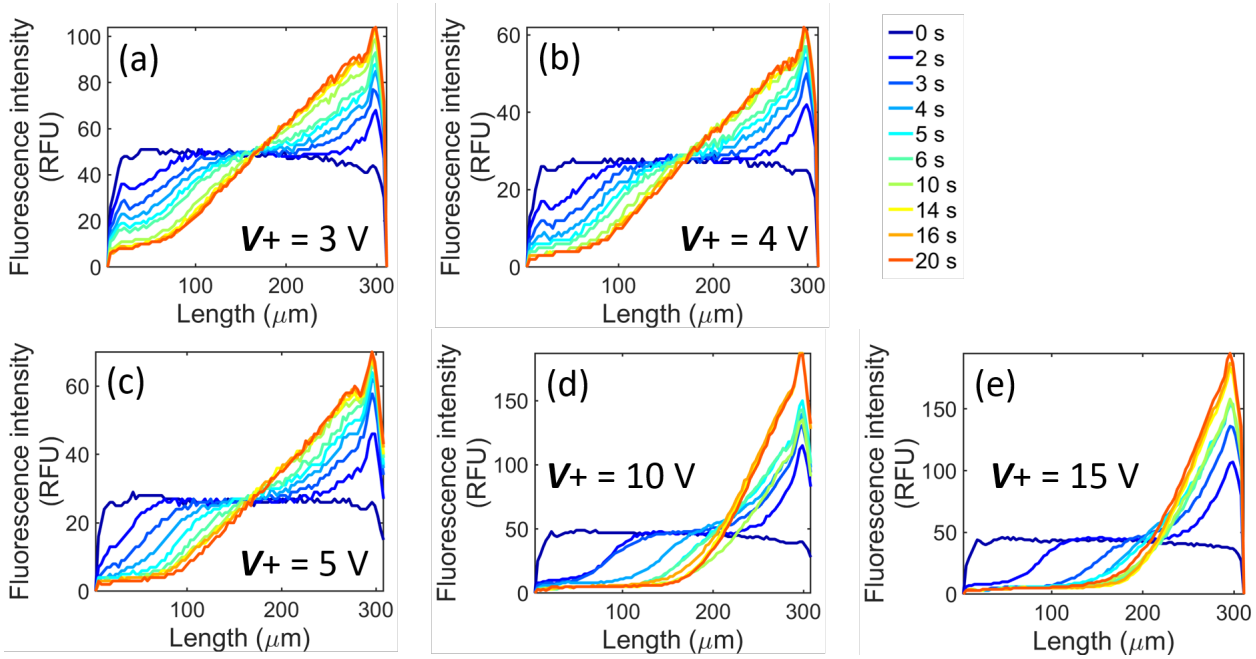

Fig. S5. Temporal evolution of the fluorescence intensity profile along the droplet centerline of a 4.6 nL droplet containing 10.0 mM phosphate buffer and 10.0 μM BODIPY^{2-}. The applied voltage bias was (a) 3.0 V, (b) 4.0 V, (c) 5.0 V, (d) 10.0 V, and (e) 15.0 V.

In-droplet separation of analytes with distinct electrophoretic mobilities. Figure S6 shows the results obtained during in-droplet ICP of two anionic tracers having higher ($BODIPY^{2-}$, green) and lower (Texas Red, red) mobility, relative to each other. In this experiment, stationary droplets comprising 10.0 μM $BODIPY^{2-}$, 100 μM Texas Red, and 90.0 mM phosphate buffer (pH 7.3) were subjected to $V+ = 100$ V (**Figure S6a,b,c,d**), and 150 V (**Figure S6e,f,g,h**), and images of green (**Figure S6b,f**) and red (**Figure S6c,g**) fluorescence were obtained after 10 s. An overlay of the brightfield images of each droplet with red and green fluorescence (**Figure S6a,e**) show three distinct regions - depletion of both dyes (bottom, cathodic end), red dye only (middle), and both dyes together (top, anodic end).

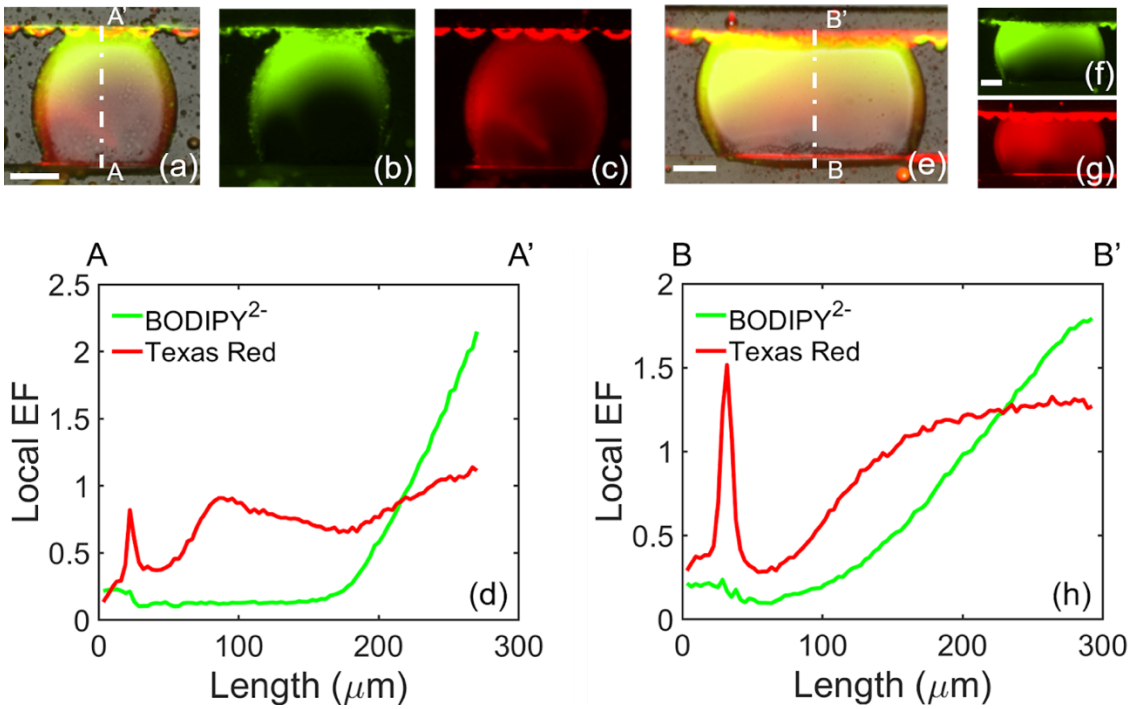

Fig. S6. In-droplet separation of analytes with distinct electrophoretic mobilities. (a and e) Overlaid of brightfield images with the fluorescence images showing the distributions of the (b and f) green tracer ($BODIPY^{2-}$) and (c and g) red tracer (Texas Red). Both droplets contained 90.0 mM phosphate buffer (pH 7.3), 10.0 μM $BODIPY^{2-}$, and 100 μM Texas Red. The droplet volumes were (a-d) 2.7 nL and (e-h) 6.6 nL, for which voltage biases were $V+ = 100$ V and 150 V, respectively. The scale bar is 100 μm. (d and h) Plots of the local degree of enrichment (local EF), along the cutlines (A-A', B-B') indicated in (a) and (d).

Cation transport into droplets. Figure S7 shows fluorescence images of the same set of three W/O droplets obtained over the time course of two successive experiments. Initially, the droplets contained 10.0 μM Rhod-2 calcium indicator dye in 10.0 mM Tris buffer. In a first experiment (right column of images) both auxiliary channels were filled with 10.0 mM Tris buffer. A voltage bias of 10.0 V was applied, and fluorescence images were obtained immediately and then at t = 10, 20, and 30 min thereafter. At t = 30 min, the voltage bias was removed, and after waiting 5 min to allow redistribution of the dye, an additional image was obtained. In a second experiment (left column of images), the solution in the anodic auxiliary was replaced with 10.0 mM $CaCl_2$. An identical voltage and image program was repeated. The fluorescence intensity of the indicator dye is increased only in the presence of $CaCl_2$. Further, the size of the IDZ is decreased in the presence of $CaCl_2$, which is attributed to decreased mobility of the indicator upon binding Ca^{2+}.

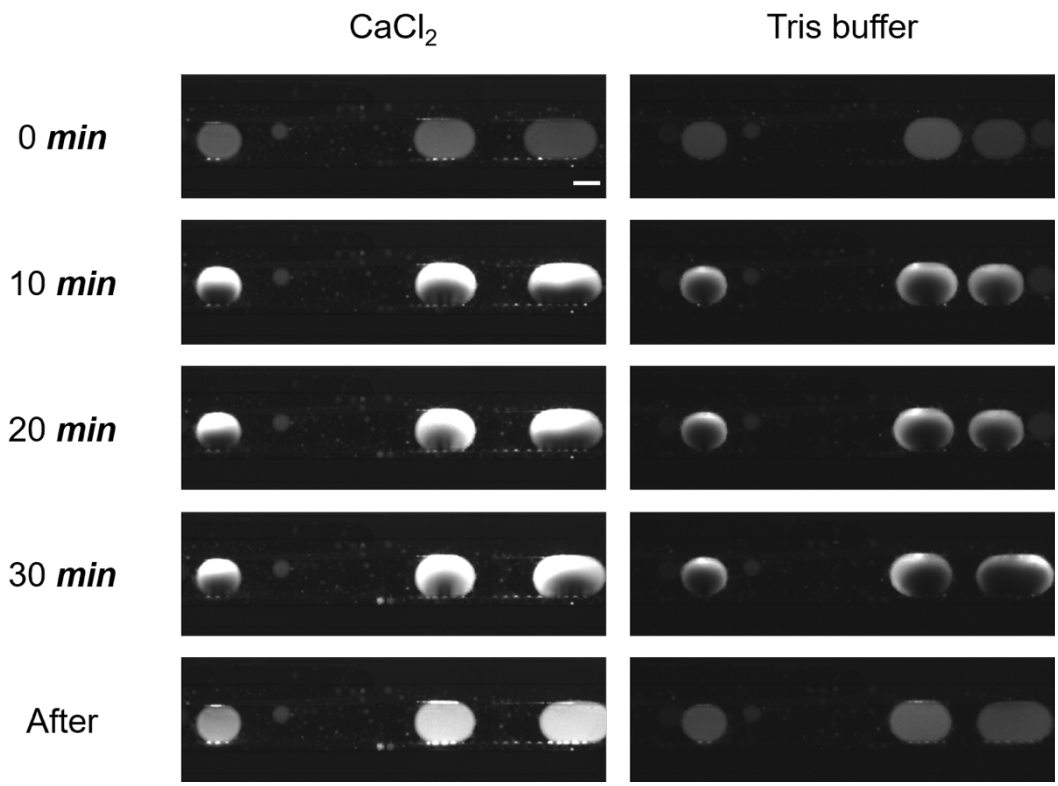

Fig. S7. Calcium injection from the auxiliary channel to the droplets. Initially, the droplet contained 10.0 mM Tris buffer and 10 μM of the calcium indicator, Rhod-2. In two successive experiments, the anodic auxiliary channel contained, first, 10.0 mM Tris buffer (right column) and 10.0 mM $CaCl_2$ (left column). In each case, following initiation of $V+ = 10.0$ V at $t = 0$ s, fluorescence images were obtained at the times indicated. An additional image was obtained 5 min after removal of the voltage bias ('After') to allow the indicator dye to become uniformly distributed.

SI References

1. Yu, M.; Hou, Y.; Zhou, H.; Yao, S. An on-demand nanofluidic concentrator. *Lab Chip* **2015**, *15*, 1524–1532.
2. Chen, C.-H.; Sarkar, A.; Song, Y.-A.; Miller, M. A.; Kim, S. J.; Griffith, L. G.; Lauffenburger, D. A.; Han, J. Enhancing Protease Activity Assay in Droplet-Based Microfluidics Using a Biomolecule Concentrator. *J. Am. Chem. Soc.* **2011**, *133*, 10368–10371.
3. Sanghavi, B. J.; Varhue, W.; Chávez, J. L.; Chou, C.-F.; Swami, N. S. Electrokinetic preconcentration and detection of neuropeptides at patterned graphene-modified electrodes in a nanochannel. *Anal. Chem.* **2014**, *86*, 4120–4125.
4. Petersson, M.; Nilsson, J.; Wallman, L.; Laurell, T.; Johansson, J.; Nilsson, S. Sample enrichment in a single levitated droplet for capillary electrophoresis. *J. Chrom. B: Biomed. Sci. Appl.* **1998**, *714*, 39–46.
5. He, M.; Sun, C.; Chiu, D. T. Concentrating solutes and nanoparticles within individual aqueous microdroplets. *Anal. Chem.* **2004**, *76*, 1222–1227.
6. Park, K.; Park, J; Jung, J. H.; Destgeer, G.; Ahmed, H.; Sung, H. J. In-droplet microparticle separation using travelling surface acoustic wave. *Biomicrofluidics* **2017**, *11*, 064112.